teins in the rafts is different in the two situations, the use of rafts as delivery vehicles and the regulation of their clustering by agrin may represent a general mechanism by which functional concentration of signaling molecules is achieved.

References and Notes

1. S. J. Singer, *Science* **255**, 1671 (1992).
2. Z. W. Hall, J. R. Sanes, *Cell* **72**, 99 (1993).
3. J. R. Sanes, J. W. Lichtman, *Annu. Rev. Neurosci.* **22**, 389 (1999).
4. M. Ferns *et al.*, *Neuron* **8**, 1079 (1992).
5. B. Malissen, A. M. Schmitt-Verhulst, *Curr. Opin. Immunol.* **5**, 324 (1993).
6. D. J. Lenschow, T. L. Walunas, J. A. Bluestone, *Annu. Rev. Immunol.* **14**, 233 (1996).
7. C. Montixi *et al.*, *EMBO J.* **17**, 5334 (1998).
8. R. G. Parton, K. Simons, *Science* **269**, 1398 (1995).
9. S. K. Bromley *et al.*, *Annu. Rev. Immunol.* **19**, 375 (2001).
10. Monoclonal antibodies were generated by W. Hoch *et al.* [*EMBO J.* **13**, 2814 (1994)] against the COOH-terminal half of agrin by immunizing several mice with an agrin fragment purified from transfected CHO cells. The binding site of the antibodies on agrin was determined by immunolabeling COS cells transfected with different agrin deletion constructs. Agrin mAb m33 has been mapped near the second laminin domain homology region and detects all agrin isoforms. Agrin m247 binds to an epitope close to splicing site Z. Agrin mAbs are commercially available through StressGen Biotechnologies, Victoria, Canada.
11. G. Tsen, W. Halfter, S. Kroger, G. J. Cole, *J. Biol Chem* **270**, 3392 (1995).
12. A. A. Khan, F. Rupp, unpublished data.
13. D. E. Mosier, *J. Immunol.* **112**, 305 (1974). The MLR was performed by using mitomycin C–treated (25 mg/ml) spleen cells from Brown Norway rats (stimulators) and splenocytes from Sprague-Dawley rats (responders).
14. C. Wülfing, M. M. Davis, *Science* **282**, 2266 (1998).
15. A. Schon, E. Freire, *Biochemistry* **28**, 5019 (1989).
16. Thymuses from 16 adult male (150 to 250 g) Sprague-Dawley rats were disassociated into single-cell suspensions in RPMI 10% fetal bovine serum (FBS). Half of the thymocyte cell suspension was untreated, and half was treated with Con A (10 μg/ml). Resting control thymocytes and thymocytes treated with Con A (10 μg/ml, 1 hour, 37°C) were washed in serum-free medium and pelleted. Cell pellets were frozen and thawed into buffer containing 50 mM Tris (pH 7.4) and protease inhibitors benzamidine (360 μg/ml), leupeptin (4 μg/ml), aprotinin (4 μg/ml), and pepstatin (4 μg/ml). Cell extracts were ground in a Dounce homogenizer and centrifuged at 35,000*g* for 45 min, and the subsequent supernatants were applied to agrin m247 and m33 immunoaffinity columns. Monoclonal agrin antibodies m33 and m247 in ascites fluid (Stressgen) were purified using Affi-Gel protein A agarose (Bio-Rad) and immobilized on Affi-Gel Hz hydrazide gel (Bio-Rad). Cell extracts were applied to the columns and washed with high-salt [phosphate-buffered saline (PBS, 0.5 M NaCl)] and low-salt (PBS, 0.15 M NaCl) buffers. Bound agrin was eluted with 0.2 M glycine-HCL, pH 2.5, and neutralized. Protein assays were performed according to directions for Pierce Coomassie blue. We used agrin's lipid raft aggregating activity to determine the multiple purification of agrin from starting thymocyte extracts to agrin immunoaffinity eluates; specific activity equivalent to agrin's lipid raft aggregating activity per amount of protein. We purified agrin 10,000-fold to homogeneity as detected by silver stain of protein resolved by SDS–polyacrylamide gel electrophoresis (SDS-PAGE). The concentration of agrin in assays was based on the molecular mass of agrin, the volume of the assay, and the amount of agrin purified from agrin immunoaffinity columns.
17. K. M. Murphy, A. B. Heimberger, D. Y. Loh, *Science* **250**, 1720 (1990).
18. Supplementary material, Web fig. 1, is available on *Science* Online at www.sciencemag.org/cgi/content/full/1056594/DC1
19. S. Lustig, D. H. Puznick, *J. Cell Physiol.* **115**, 87 (1983).
20. N. Razi, A. Varki, *Proc. Natl. Acad. Sci.* **95**, 7469 (1998).
21. A. Viola, S. Schroeder, Y. Sakakibara, A. Lanzavecchia, *Science* **283**, 680 (1999).
22. M. L. Dustin, A. C. Chan, *Cell* **103**, 283 (2000).
23. M. Gunzer *et al.*, *Immunity* **13**, 323 (2000).
24. M. Demetriou, M. Granovsky, S. Quaggin, J. W. Dennis, *Nature* **409**, 733 (2001).
25. G. Lück, W. Hoch, C. Hopf, D. Blottner, *Mol. Cell. Neurosci.* **16**, 269 (2000).
26. Splenocytes from eight adult male (150 to 250 g) Sprague-Dawley rats were isolated by Ficoll-hypaque and cultured in RPMI 10% FBS. Half of the splenocyte cell suspension was untreated, and half was treated with Con A (10 μg/ml). Resting control splenocytes and splenocytes treated with Con A (10 μg/ml, 1 hour, 37°C) were washed in serum-free medium and pelleted. Cell pellets were frozen and thawed into buffer containing 50 mM Tris (pH 7.4), and protease inhibitors benzamidine (360 μg/ml), leupeptin (4 μg/ml), aprotinin (4 μg/ml), and pepstatin (4 μg/ml). After centrifugation at 800*g* at 4°C for 10 min, the postnuclear supernatant was incubated with Triton X-100 at a final concentration of 1% for 30 min at 4°C. The lysate was adjusted to 1.3 M sucrose, placed at the bottom of a step sucrose gradient (0.2 to 0.9 M), and centrifuged (38,000 rpm, 15 hours).

27. We thank C. Hopf, R. Schnaar, and S. H. Snyder for critically reviewing the manuscript, R. Tracey, Registered Biological Photographer, for graphic art, and M. Khan for insightful discussions. This work was supported in part by grants from the E. A. and J. Klingenstein Fund (F.R.), the Council for Tobacco Research (F.R.), and from the NIAID (R01AI20922 to M.J.S.).

16 October 2000; accepted 25 April 2001
Published online 10 May 2001;
10.1126/science.1056594
Include this information when citing this paper.

Evidence for Dust Grain Growth in Young Circumstellar Disks

Henry B. Throop,[1]* John Bally,[2] Larry W. Esposito,[1] Mark J. McCaughrean[3]

Hundreds of circumstellar disks in the Orion nebula are being rapidly destroyed by the intense ultraviolet radiation produced by nearby bright stars. These young, million-year-old disks may not survive long enough to form planetary systems. Nevertheless, the first stage of planet formation—the growth of dust grains into larger particles—may have begun in these systems. Observational evidence for these large particles in Orion's disks is presented. A model of grain evolution in externally irradiated protoplanetary disks is developed and predicts rapid particle size evolution and sharp outer disk boundaries. We discuss implications for the formation rates of planetary systems.

The growth of dust grains orbiting young stars represents the first stage of planet formation (*1*). However, stars born in massive star-forming regions such as the Orion nebula are heated by intense ultraviolet (UV) radiation from nearby O and B stars, and the gas and dust in their disks can be lost in less than 10^5 years (*2*). Planet formation in such environments may therefore be inhibited if it requires substantially longer time than this (*3*). But, if growth to large particles can occur before removal of the gas and small particles, planets may nevertheless form from these disks. In this report, visual and near-infrared (IR) wavelength images obtained with the Hubble Space Telescope (HST) are used to show that particles in Orion's largest disk have grown to radii larger than 5 μm. Furthermore, the absence of millimeter-wavelength emission may provide evidence that grains have grown to sizes larger than a few millimeters. We develop a grain evolution model incorporating the effects of photoablation that demonstrates that the time scale for grain growth can be shorter than the photoevaporation time. It is thought that the majority of stars in the Galaxy form in photoevaporating regions such as the Orion nebula (*4*); if this is true, then giant planets and Kuiper belts of icy bodies around stars are probably rare unless they are formed very rapidly.

Solar system–sized circumstellar disks in the Orion nebula were first inferred from radio observations of dense ionized regions surrounding young low-mass stars (*5*). HST

[1]Laboratory for Atmospheric and Planetary Sciences, University of Colorado, Boulder, CO 80309–0392, USA. [2]CASA, University of Colorado, Boulder, CO 80309–0389, USA. [3]Astrophysikalisches Institut Potsdam, An der Sternwarte 16, D-14482 Potsdam, Germany.

*Present address: Southwest Research Institute, 1050 Walnut Street, Suite 426, Boulder, CO 80302, USA. E-mail: throop@boulder.swri.edu

subsequently yielded images of extended circumstellar material surrounding over half of the observed 300 young low-mass stars in the core of the Orion nebula (*6*, *7*). Most of these "proplyds" consist of comet-shaped ionized envelopes pointing directly away from the brightest stars in the nebula (*8*, *9*). Proplyds are believed to contain evaporating circumstellar disks (*10*), and over 40 disks have been resolved on HST images. More than 25 are found inside ionized envelopes, whereas 15 are seen purely in silhouette against the background light of the nebula.

Assuming disk masses of ~0.01 to 0.05 $M_\odot$ (1 $M_\odot$ = 1 solar mass) (*10*), external radiation erodes disks in the central 1 pc of the Orion nebula on 10^4- to 10^5-year time scales (*3*, *10*). Soft UV photons (91 nm < λ < 200 nm) from nearby massive stars heat the disk surface layers to about 1000 K. Gas heated above the local escape velocity is lost from the disk at loss rates of $M \approx 10^{-7}$ to 10^{-6} $M_\odot$ year^{-1} (*2*, *10*) and forms the cometary proplyds surrounding many of Orion's young stars. Dust grains will be entrained in the escaping neutral outflow where the gas drag forces on them exceed the force of gravity; the small ionized outflow component has negligible effect on grain loss (*11*). Entrained dust has been observed just inside the ionization fronts in several proplyds (*9*) but has not been considered in previous modeling.

The properties of the grains in Orion's circumstellar disks can be probed by the wavelength dependence of the attenuation of the background nebular light that filters through the translucent disk edges. Standard interstellar (*12*) grains with radii of 0.1 to 0.2 μm (*13*) scatter shorter wavelength visible light more efficiently than longer wavelengths. Therefore, disks containing predominantly small interstellar grains become more transparent with increasing wavelength. On the other hand, the opacity of disks containing predominantly large grains (larger than several times the wavelength) will be independent of the wavelength. Although small grains "redden" transmitted light, large grains do not alter its color, rendering the translucent portion of the disk "gray."

The largest circumstellar disk in the Orion nebula, 114-426, is seen in silhouette against background nebular light. This nearly edge-on disk (the central star is occulted by the disk) has a radius of ~550 astronomical units (AU) and a resolved translucent outer edge roughly 200 by 200 AU in size at its northeast ansa (Fig. 1) (*9*). Grain properties in this region can be probed by the attenuation of the bright background 1870-nm Paschen α and 656-nm Hα lines. Because both these lines originate from recombinations of ionized hydrogen, the brightness ratio between these two lines is relatively constant over the extent of 114-426.

We used the Planetary Camera of HST's WFPC2 instrument to obtain a set of four dithered 400-s Hα exposures of 114-426 on 11 January 1999, resulting in reduced images with an angular resolution of 0.07 arc sec, or 30 AU (*9*). We also used HST's NICMOS1 camera to obtain a 640-s Paschen α exposure on 26 February 1998 at resolution of 0.16 arc sec (*14*). To compare these images at identical resolutions, we convolved the Hα image with a synthetic Paschen α point-spread function (PSF) and the Paschen α image with an Hα PSF.

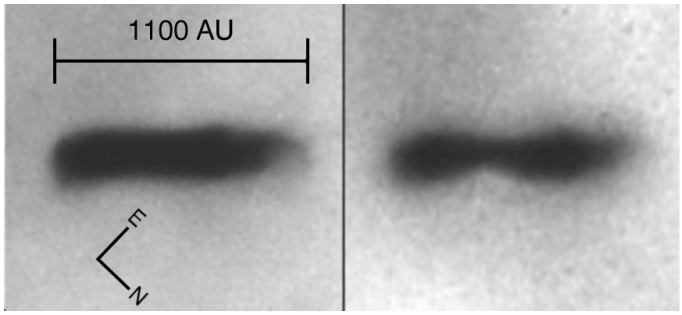

Fig. 1. Images of the 114-426 disk in Orion at 656 nm (left) and 1870 nm (right) obtained with HST. The images have been rotated and scaled to the same spatial scale and are shown at full resolution before convolving as described in the text. The maximum and minimum background intensities have been normalized to unity and zero, respectively. Both images were processed and calibrated through the standard HST data pipeline.

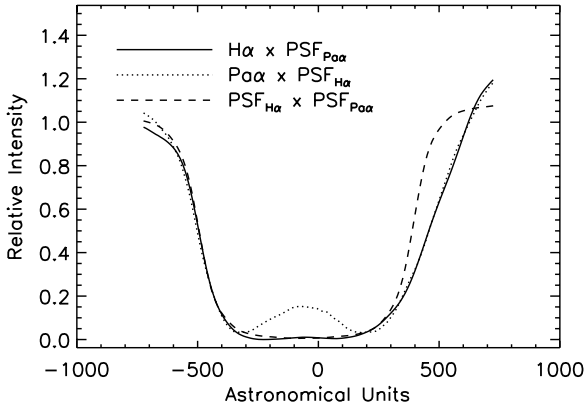

Fig. 2. One-dimensional intensity slices along the major axis of the 114-426 circumstellar disk. Both images have been convolved with their complementary PSFs to produce images at matched angular resolutions. The dashed line is the result of convolving a sharp-edged disk with both PSFs. The disk's southwest ansa is consistent with a sharp disk edge. In contrast, the disk's translucent northeast ansa is spatially extended over at least four resolution elements. The indistinguishable profiles at the two wavelengths indicate that transmission through the translucent portion of the disk is achromatic and the disk is dominated by particles larger than 5 μm.

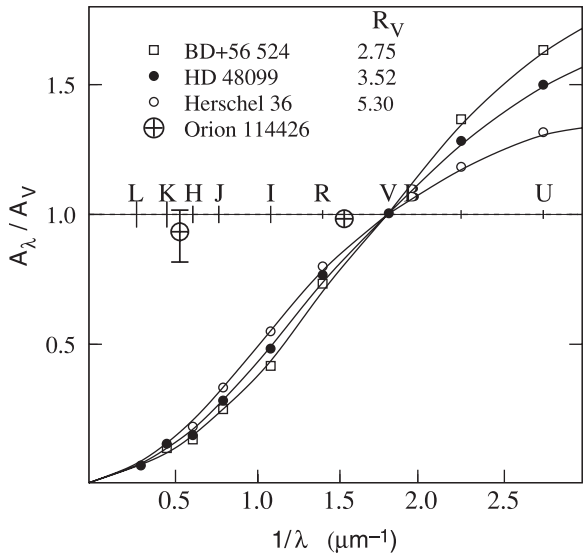

Fig. 3. The wavelength dependence of the light transmitted through the translucent portion of the 114-426 disk, compared with the range of standard observed interstellar reddening laws. The 656- and 1870-nm data points for the northeast ansa of 114-426 are marked. All data have been normalized to the V photometric band. The points for 114-426 show that the extinction is gray and cannot be represented by any interstellar extinction law. The error bar on the 1870-nm point shows 3σ errors, dominated by spatial variations in the background light at both wavelengths and flat-field artifacts in the 1870-nm image. *A* indicates the extinction in magnitudes at wavelength λ. The color ratio R_v is defined as $A_v/(A_v - A_B)$. Other single letters indicate the standard photometric bands. The stellar data were taken from (*30*).

Linear slices through the disk midplane at 656 nm and 1870 nm show that the opacity profiles of the translucent western edge of 114-426 are indistinguishable (Fig. 2). Thus, background light is not reddened; dust at the disk edge is gray to a level of ~5% between 656 and 1870 nm. The mean extinction of the translucent ansa of the 114-426 disk at these wavelengths can be compared with the reddening produced by observations of interstellar grains in several typical regions (Fig. 3). The 114-426 disk's translucent edge is achromatic and cannot be fit by any standard interstellar extinction law. The standard interstellar extinction curve indicates that the opacity should be 5 to 10 times lower at 1870 nm than at 656 nm. This result depends only weakly on composition, grain shape, or the presence of fractal aggregates (*15*, *16*). The observed gray opacity indicates that extinction is dominated by particles larger than 5 μm in radius, 25 to 50 times larger than typical interstellar grains. In contrast to the northeast ansa, the disk's polar halo region decreases in size with wavelength, indicating a suspended population of small particles above the disk poles (*14*). Although previous observations of 114-426 (*8*) indicated a decrease in disk size by 20% from 656 to 1870 nm, that result may have reflected poor signal/noise ratio in the earlier 1870-nm observations (*11*).

The lack of millimeter-wavelength emission places additional constraints on grain sizes. We observed six Orion nebula disks, including 114-426, with the Owens Valley Radio Observatory (OVRO) millimeter-wavelength interferometer at $\lambda = 1.3$ mm continuum (*17*). None were detected, implying mass limits of $M_{disk} < 0.020\ M_\odot$ under the assumption of an interstellar emissivity of 2×10^{-2} cm^2 g^{-1} (*18*). However, in revisiting our analysis of these data, we note the possibility that grains have grown larger than a few millimeters and thus the standard emissivity may underestimate the mass. The models described below predict that particles grow to larger than 1 mm throughout the disk in less than 10^5 years, causing an emissivity of 2×10^{-3} cm^2 g^{-1} and implying disk masses as large as 0.2 $M_\odot$.

We have developed a numerical model (*11*) to explore grain behavior within photoevaporating disks. Our model includes (i) grain growth due to mutual collisions and accumulation of ice mantles (*19*), (ii) coupling and loss of small grains entrained in UV photoevaporation-induced outflow (*3*, *10*), and (iii) photosputtering of ices (*20*). The grain density is assumed to remain constant as grains collide and stick within turbulent eddies produced by heat escaping from the disk midplane. Vertical and azimuthal symmetry is assumed (*21*), and the abundance and size distribution of ice, silicate, and gas are tracked separately at each time step. Our disk has an initial mass of 0.1 $M_\odot$, with a grain size distribution identical to interstellar dust. The model starts when the ionizing source turns on and stops when the disk thermal optical depth has dropped below unity and can no longer sustain convection (*19*), typically in a little over 10^5 years. After convection stops, grain growth is dominated by processes such as settling and gravitational interactions. These processes are not considered here. The model does not simulate 114-426 in its current, nonphotoevaporating state (*22*); rather, it simulates the 114-426 disk as it would appear placed near the Orion nebula core at a distance of 0.1 pc.

Grains grow most rapidly in the center of the model disk (Fig. 4A), where the highest densities and temperatures are found and photoevaporation does not operate. The growth rate decreases with distance from the central star; grain sizes reach $r = 1$ m at 10 AU and $r = 1$ mm at 500 AU in 10^5 years. In the outer disk, small (<1 mm) grains are entrained in the photoevaporative flow from the disk surface and lost from the system, decreasing the optical depth (Fig. 4B). After 10^5 years, few particles remain in the disk outward of 40 AU. At the transition between these "grain growth" and "grain loss" regimes, an edge populated by large, centimeter-sized particles is left behind. After the silicate population has stabilized, photosputtering continues to reduce ice particle sizes and remove gas, and nearly all ice and gas are removed by 10^6 years. Only silicates that grow large enough ($r > 1$ mm) to resist photoevaporative entrainment are retained. Ices do not survive and only rocky planets, planetary cores, or asteroids can form.

In the standard planetary formation model, giant planets such as Jupiter form by

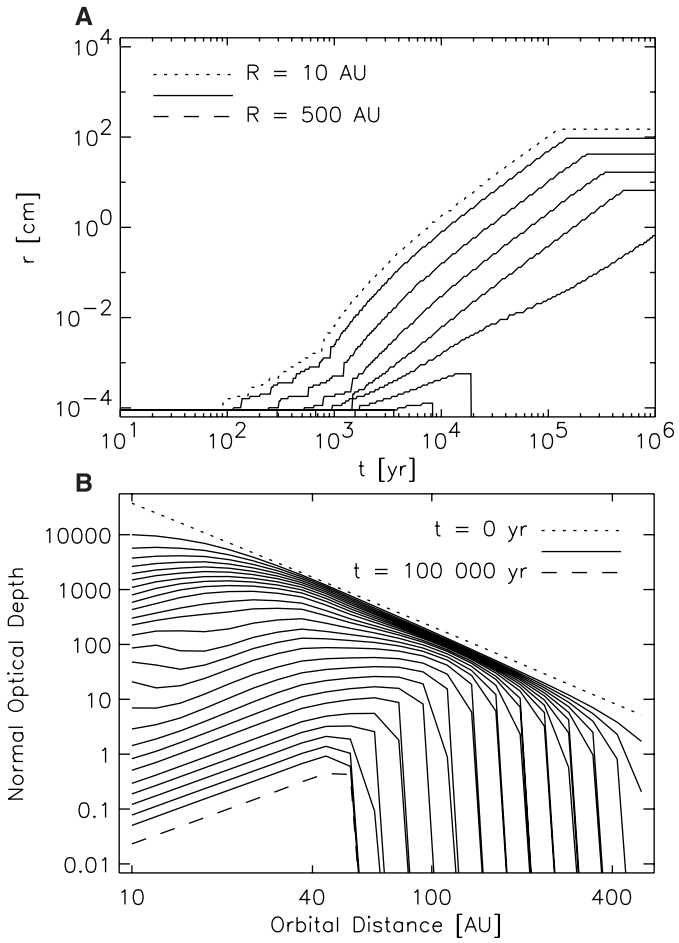

Fig. 4. A model for grain growth in a photoevaporating circumstellar disk exposed to a UV radiation field typical of the Orion nebula. The initial grain size distribution is that of interstellar dust. (**A**) The evolution of the particle size with time at several radial distances. Solid lines correspond to radial distances $R_i = \exp(2.31 + 0.43n_i)$ AU. The outermost several bins do not grow substantially, and their lines appear superimposed on each other. Particles grow quickly at the inner edge because of high collision velocities, high gas densities, and slow loss processes. Growth is terminated when IR optical depth drops below unity, inhibiting convection. (**B**) The evolution of the radial profile of the disk's opacity as viewed from the disk axis. Grains at the outer edge are removed by the photoablation flow, whereas grains in the inner disk grow rapidly. These two processes create a disk populated by large particles. Time steps for the solid lines correspond to times $t_i = \exp(5.1 + 0.24n_i)$ years. The input parameters used here are representative of photoevaporative conditions 0.1 pc from the Orion nebula core (*10*, *31*). The following disk parameters are assumed: The surface density declines with disk radius as $\Sigma \sim R^{-3.5}$ (*32*), the vertical height scales as $z = R/10$, the sputtering rate is given by $(dr/dt)_s = 1$ μm year^{-1}, and the sticking efficiency is $\epsilon = 0.1$. The outflow column density is $n_0 = 3 \times 10^{22}$ cm^{-2}, higher than the 3×10^{21} cm^{-2} of (*31*) to account for deeper UV penetration due to the large grains in the disk. The viscosity parameter is $\alpha = 10^{-2}$, the outflow temperature at its base is $T_o = 1000$ K, the central star mass is $M_s = 1\ M_\odot$, the disk inner and outer radii are $R_{in} = 10$ AU and $R_{out} = 500$ AU, and the grain density is $\rho = 1$ g cm^{-3}.

accreting hydrogen- and helium-rich gas from the disk onto a large rocky core (*23*). In Orion-like environments, there may not be time to grow the requisite cores before loss of the gas because Jupiter's formation would require 10^6 to 10^7 years. If giant planets form in Orion-like systems, they must do so before disk photoevaporation. One viable mechanism for rapid formation of giant planets is gravitational collapse, which has been modeled to occur in disks with $M_{\rm disk} > 0.13\ M_\odot$ on 10^3-year time scales around solar-mass stars (*24*). Icy Kuiper belt objects and comets are believed to have formation time scales of 10^8 to 10^9 years (*25*). Thus, these objects are also difficult to form in Orion-like environments. The architectures of any new planetary systems that might form in Orion are likely to be different from that of our solar system.

The evidence for large particles in 114-426 complements several previous studies of particles in young disks. The reflected-light near-IR spectrum of the disk orbiting HR4796A (*26*) provides evidence for particles with radii larger than 2 to 3 μm. Several disks in NGC2024 (*27*) and Taurus (*28*) reveal relatively flat submillimeter spectra that may indicate large grains. However, near-IR observations of the disk in HH30 (*29*) show normal dust opacities and no evidence for grain growth, and sub-mm observations of the HL Tau disk (*1*) are inconclusive. Grain growth in disks appears to depend strongly on their environment.

The majority of young stars in the Milky Way Galaxy appear to have formed in large, dense clusters such as the Orion nebula, rather than in smaller, dark clouds such as Taurus-Auriga (*4*). Within large clusters, the majority of stars form near massive stars where their disks can be rapidly destroyed. Thus, planet formation models must be revised to consider the destructive effects of these environments. We present evidence for large gains in one Orion disk. This creates the possibility that planetary system with architectures different from our own solar system may nonetheless form in such hazardous environments.

References and Notes

1. S. V. W. Beckwith, T. Henning, Y. Nakagawa, in *Protostars and Planets IV*, V. Mannings, A. P. Boss, S. S. Russell, Eds. (Univ. of Arizona Press, Tucson, AZ, 2000), pp. 533–558.
2. C. J. Henney, C. R. O'Dell, *Astron. J.* **118**, 2350 (1999).
3. H. Stoerzer, D. Hollenbach, *Astrophys. J.* **495**, 853 (1998).
4. F. M. Walter, J. M. Alcala, R. Neuhauser, M. Sterzik, S. J. Wolk, in *Protostars and Planets IV*, V. Mannings, A. P. Boss, S. S. Russell, Eds. (Univ. of Arizona Press, Tucson, AZ, 2000), pp. 273–298.
5. E. Churchwell, M. Felli, D. O. S. Wood, M. Massi, *Astrophys. J.* **321**, 516 (1987).
6. C. R. O'Dell, Z. Wen, X. Hu, *Astrophys. J.* **410**, 696 (1993).
7. M. J. McCaughrean, C. R. O'Dell, *Astron. J.* **111**, 1977 (1996).
8. M. J. McCaughrean *et al.*, *Astrophys. J.* **492**, L157 (1998).
9. J. Bally, C. R. O'Dell, M. J. McCaughrean, *Astron. J.* **119**, 2919 (2000).
10. D. Johnstone, D. Hollenbach, J. Bally, *Astrophys. J.* **499**, 758 (1998).
11. H. B. Throop, thesis, University of Colorado, Boulder (2000).
12. The term "interstellar" refers to the population of small, primordial dust grains in the Orion nebula that have not been processed in a circumstellar disk.
13. S.-H. Kim, P. G. Martin, P. D. Hendry, *Astrophys. J.* **422**, 164 (1994).
14. M. J. McCaughrean, K. R. Stapelfeldt, L. M. Close, in *Protostars and Planets IV*, V. Mannings, A. P. Boss, S. S. Russell, Eds. (Univ. of Arizona Press, Tucson, AZ, 2000), pp. 485–507.
15. K. Lumme, J. Rahola, J. W. Hovenier, *Icarus* **126**, 455 (1997).
16. M. I. Mishchenko, L. D. Travis, D. W. Mackowski, *J. Quant. Spec. Rad. Trans.* **55**, 535 (1996).
17. J. Bally, L. Testi, A. Sargent, J. Carlstrom, *Astron. J.* **116**, 854 (1998).
18. L. G. Mundy, L. W. Looney, E. A. Lada, *Astrophys. J.* **452**, L137 (1995).
19. H. Mizuno, W. J. Markiewicz, H. J. Voelk, *Astron. Astrophys.* **195**, 183 (1988).
20. M. S. Westley, R. A. Baragiola, R. E. Johnson, G. A. Baratta, *Nature* **373**, 405 (1995).
21. B. Dubrulle, G. Morfill, M. Sterzik, *Icarus* **114**, 237 (1995).
22. 114-426 is thought to show no photoevaporation because it is outside the Orion core's Strömgren sphere and thus receives no soft UV flux; we note the possibility that it may not be photoevaporating today because all gas has already been lost in previous photoevaporative episodes and it is a pure dust disk.
23. J. B. Pollack *et al.*, *Icarus* **124**, 62 (1996).
24. A. P. Boss, *Science* **276**, 1836 (1997).
25. P. Farinella, D. R. Davis, S. A. Stern, in *Protostars and Planets IV*, V. Mannings, A. P. Boss, S. S. Russell, Eds. (Univ. of Arizona Press, Tucson, AZ, 2000), pp. 1255–1282.
26. G. Schneider *et al.*, *Astrophys. J. Lett.* **513**, 127 (1999).
27. A. E. Visser, J. S. Richer, C. J. Chandler, R. Padman, *Mon. Not. R. Astron. Soc.* **301**, 585 (1998).
28. V. Mannings, J. P. Emerson, *Mon. Not. R. Astron. Soc.* **267**, 361 (1994).
29. A. M. Watson, K. R. Stapelfeldt, J. E. Krist, C. J. Burrows, in preparation.
30. J. A. Cardelli, G. C. Clayton, J. S. Mathis, *Astrophys. J.* **345**, 245 (1989).
31. H. Stoerzer, D. Hollenbach, *Astrophys. J.* **515**, 669 (1999).
32. H. W. Yorke, P. Bodenheimer, G. Laughlin, *Astrophys. J.* **411**, 274 (1993).

33. This research was funded by the Cassini project; the NASA Astrobiology Institute (grant NCC1-1052); NASA grants NAG5-8108, GO-07367.01-A, and GO-06824.01-A; Deutsches Zentrum für Luftund Raumfahrt (DLR) grant number 50-OR-0004; and European Commission Research Training Network RTN1–1999–00436. We thank C. Campbell, N. Turner, and two anonymous reviewers for their comments.

17 January 2001; accepted 20 April 2001
Published online 26 April 2001;
10.1126/science.1059093
Include this information when citing this paper.

Observation of a Train of Attosecond Pulses from High Harmonic Generation

P. M. Paul,[1] E. S. Toma,[2] P. Breger,[1] G. Mullot,[3] F. Augé,[3] Ph. Balcou,[3] H. G. Muller,[2]* P. Agostini[1]

In principle, the temporal beating of superposed high harmonics obtained by focusing a femtosecond laser pulse in a gas jet can produce a train of very short intensity spikes, depending on the relative phases of the harmonics. We present a method to measure such phases through two-photon, two-color photoionization. We found that the harmonics are locked in phase and form a train of 250-attosecond pulses in the time domain. Harmonic generation may be a promising source for attosecond time-resolved measurements.

The advent of subfemtosecond or attosecond (as) light pulses will open new fields of time-resolved studies with unprecedented resolution. Just as subpicosecond or femtosecond (fs) pulses have allowed the resolution of molecular movements, attosecond pulses may enable us to resolve electronic dynamics. Several groups around the world are researching the generation of subfemtosecond pulses. Large bandwidths are required to support such pulses. The spectrum of a 200-as unipolar pulse covers the optical spectrum from the near infrared to the extreme ultraviolet. There are two known kinds of sources with the potential to produce coherent radiation over such bandwidths: high harmonic generation (HHG) (*1*) and stimulated Raman scattering (*2, 3*). Both methods have, in theory, a tendency to produce a train of closely spaced pulses rather than a single pulse. Even such trains of attosecond pulses, applied to experiments, can open a new field of attosecond physics, allowing the study of processes of unprecedented speed. Moreover, methods of selecting only one pulse from the train have already been suggested (*4*). The present experimental study focuses on HHG and demon-

[1]Commissariat à l'Energie Atomique DRECAM/SPAM, Centre d'Etudes de Saclay, 91191 Gif-sur-Yvette, France. [2]FOM–Institute for Atomic and Molecular Physics, Kruislaan 407, 1098 SJ, Amsterdam, Netherlands. [3]Laboratoire d'Optique Appliquée, École Nationale Supérieure de Techniques Avancées (ENSTA)–Ecole Polytechnique, CNRS UMR 7639, 91761 Palaiseau Cedex, France.

*To whom correspondence should be addressed. E-mail: muller@amolf.nl